Chapter 3

Non-Invasive Microwave Characterization of Dielectric Scatterers

Sandra Costanzo, Giuseppe Di Massa,
Matteo Pastorino, Andrea Randazzo and Antonio Borgia

Additional information is available at the end of the chapter

http://dx.doi.org/10.5772/50842

1. Introduction

Microwave tomography is a technique aimed at inspecting unknown bodies by using an incident radiation generated at microwave frequencies (Ali & Moghaddam, 2010; Bellizzi, Bucci, & Catapano, 2011; Catapano, Crocco, & Isernia, 2007; Chen, 2008; Ferraye, Dauvignac, & Pichot, 2003; Gilmore, Mojabi, & LoVetri, 2009; Habashy & Abubakar, 2004; Isernia, Pascazio, & Pierri, 2001; Kharkovsky & Zoughi, 2007; Lesselier & Bowler, 2002; Litman, Lesselier, & Santosa, 1998; Oliveri, Lizzi, Pastorino, & Massa, 2012; Pastorino, 2010; Rekanos, 2008; Schilz & Schiek, 1981; Shea, Kosmas, Van Veen, & Hagness, 2010; Zhang & Liu, 2004; Zhou, Takenaka, Johnson, & Tanaka, 2009). An illuminating system (Costanzo & Di Massa, 2011; Paulsen, Poplack, Li, Fanning, & Meaney, 2000; Zoughi, 2000) is used to produce the incident waves that interact with the body to produce a scattered electromagnetic field. Another system is used to acquire the measurements that are used as input values for the reconstruction procedures. These values are the field samples resulting from the sum of the incident and scattered waves. Since the incident field (i.e., the field produced by the illuminating system when the object is not present) is a known quantity, the scattered electric field can be obtained by a direct subtraction. Moreover, the scattering field is related to the properties of the unknown body by well-known key relationships. In particular, both position, shape and dielectric parameters of the target affect the scattered field. In this Chapter, we consider the inspection of (possibly inhomogeneous) dielectric targets, which are characterized by the distributions of the dielectric permittivity and electric conductivity, whereas magnetic materials (e.g., materials for which the magnetic permittivity is different from the vacuum one) are not considered (El-Shenawee, Dorn, & Moscoso, 2009; Franchois & Pichot, 1997). The relationship between the target properties and the sampled scattered electric field is, in integral form, a Fredholm equation of the first kind, usually indicated as the "data equation" (Bucci, Cardace, Crocco, & Isernia, 2001; Rocca, Benedetti, Donelli,

Franceschini, & Massa, 2009; van den Berg & Abubakar, 2001). The kernel of this equation is the Green's function for two dimensional geometries in free space (in this Chapter we consider imaging configurations in free space, although other configurations - e.g., half space imaging - could be assumed by introducing the proper Green's function for the specific configuration). The considered problem belongs to the class of inverse problems, which are usually ill-posed, in the sense that the solution can be not unique and unstable. To face the ill-posedness of the problem, the "data equation" is often solved together with the so-called "state equation", relating the incident electric field inside the inspected object to the problem unknowns. In particular, in the developed approach, the two equations are combined together and a single nonlinear equation is obtained. In order to numerically solve the inverse problem, a discretization is usually necessary. A pixelated image of the scattering cross section can be obtained by using square pulse basis functions. The discrete nature of the measurements (we assume that each measurement antenna is able to collect the field at a given point inside a fixed observation domain) is equivalent to consider Dirac delta functions as testing function. The result of the discretization is a (nonlinear) system of equations to be solved, usually very ill-conditioned. In order to solve, in a regularized sense, the inverse scattering problem in the discrete setting, an iterative algorithm based on an inexact-Newton method is applied (Bozza, Estatico, Pastorino, & Randazzo, 2006; Estatico, Bozza, Massa, Pastorino, & Randazzo, 2005).

The reconstruction method proposed in this Chapter can be, in principle, applied to a large variety of dielectric objects, having homogeneous or multilayer cross-sections with arbitrary shape. Only for demonstration purpose, a simple homogeneous reference target of known dielectric properties is assumed in the following. The scattered field is acquired, both in amplitude and phase, on a square investigation domain around the target, sufficiently extent to be within the radiating near-field region (Costanzo & Di Massa, 2011). The incident field, oriented along the cylindrical target axis, is produced by a standard horn antenna, and a probe of the same kind is used to collect the field on the acquisition domain, for different positions of the illuminating horn. The measured scattered field data are subsequently processed to solve the inverse scattering problem and successfully retrieve the dielectric profile of the target under test.

The Chapter is organized as follows. In Section 2, a detailed mathematical description of the reconstruction method and the relative solving procedure are provided. The imaging setup configuration and the performed scattering measurements are discussed in Section 3. Some preliminary results concerning the inversion of measured data are reported in Section 4. Finally, conclusions are outlined in Section 5.

2. Mathematical formulation

The considered approach assumes tomographic imaging conditions and it aims at reconstructing the distributions of the dielectric properties of a slice of the target (Fig. 1). A transmitting (TX) antenna is successively positioned in S different locations $\mathbf{r}_s^{TX}$, $s = 1, \ldots, S$, and generates a set of known z-polarized incident waves, whose electric field vectors can be expressed as:

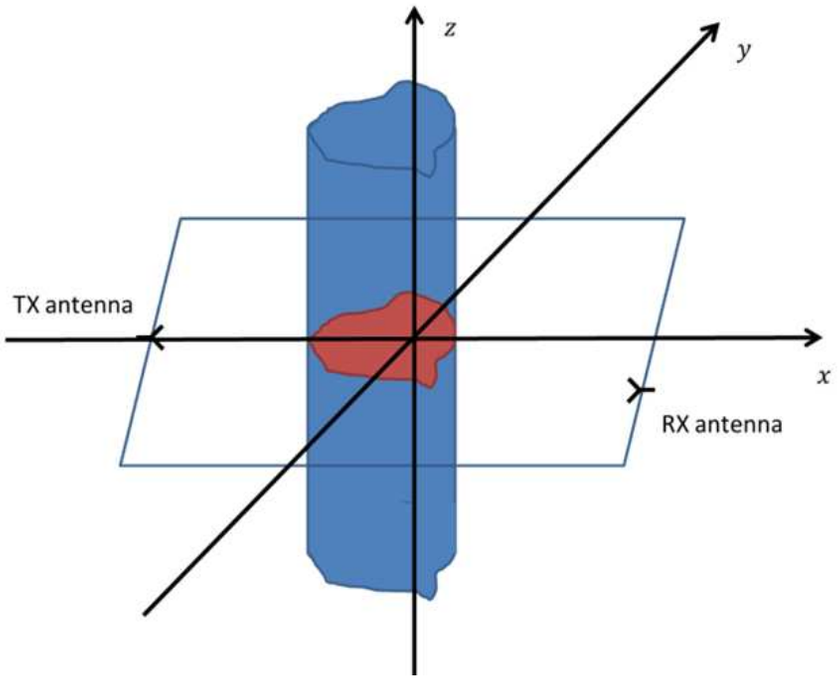

Figure 1. Schematic representation of the considered tomographic configuration

$$\mathbf{E}_{inc}^{s}(\mathbf{r},\omega) = e_{inc}^{s}(x,y,\omega)\hat{\mathbf{z}} \tag{1}$$

where ω is the angular working frequency. It should be noted that the proposed approach does not require plane wave illumination of the target.

The object is assumed to have cylindrical geometry, with the cylindrical axis directed along a direction parallel to the electric field vectors of the incident electric field (i.e., the z axis). Moreover, the dielectric properties are assumed to be independent from the z coordinate, i.e., $\epsilon(\mathbf{r}) = \epsilon(x,y)$ and $\sigma(\mathbf{r}) = \sigma(x,y)$, being ϵ and σ the dielectric permittivity and the electric conductivity, respectively.

The object interacts with the impinging electric field. From the above hypotheses it results that the resulting total electric field is z-polarized, too, and it can be written as:

$$\mathbf{E}_{tot}^{s}(\mathbf{r},\omega) = e_{tot}^{s}(x,y,\omega)\hat{\mathbf{z}} = e_{scatt}^{s}(x,y,\omega)\hat{\mathbf{z}} + e_{inc}^{s}(x,y,\omega)\hat{\mathbf{z}} \tag{2}$$

where $e_{scatt}^{s}(x,y,\omega)$ is the *scattered* electric field (due to the sth illumination), which is a mathematical quantity taking into account for the interaction effect between the incident electric field and the target. The total electric field is measured, for any location of the transmitting antenna, by a receiving (RX) antenna successively positioned in M points $\mathbf{r}_{s,m}^{RX}$, $s = 1,\dots,S,\ m = 1,\dots,M$.

From a mathematical point of view, the relationship between the measured total electric field and the dielectric properties of the target can be modeled by using a Lippmann-Schwinger equation (Pastorino, 2010), i.e.,

$$e_{tot}^{s}(x,y,\omega) = e_{inc}^{s}(x,y,\omega) + j\frac{k_0^2}{4}\int_D \tau(x',y')\, e_{tot}^{s}(x',y',\omega) H_0^{(2)}(k_0\rho)dx'dy',\ s = 1,\dots,S \tag{3}$$

where $k_0 = \omega\sqrt{\epsilon_0\mu_0}$ is the free-space wavenumber (being ϵ_0 and μ_0 the dielectric permittivity and the magnetic permeability of the vacuum, respectively). In equation (3), $H_0^{(2)}$ is the Hankel function of zero-th order and second kind, $\rho = \sqrt{(x-x')^2 + (y-y')^2}$, and τ denotes the *contrast function*, which is defined as:

$$\tau(x,y) = \epsilon(x,y) - \frac{j\sigma(x,y)}{\omega\epsilon_0} - 1 \tag{4}$$

The imaging procedure, starting from the measured samples of the total electric field in the $S \times M$ measurement locations, is aimed at retrieving the contrast function, which contains all information about the unknown distributions of the dielectric properties. Consequently, equation (3) is discretized (by using pulse basis function to represent the unknowns (Richmond, 1965)) and computed at the measurement positions, leading to the following set of discrete equations:

$$\mathbf{e}_{scatt}^{s} = \mathbf{H}^{s}\mathrm{diag}(\boldsymbol{\tau})\mathbf{e}_{tot}^{s},\ s = 1, \dots, S \tag{5}$$

where:

$$\mathbf{e}_{scatt}^{s} = \begin{bmatrix} e_{scatt}^{s}\left(x_{s,1}^{RX}, y_{s,1}^{RX}, \omega\right) \\ \vdots \\ e_{scatt}^{s}\left(x_{s,M}^{RX}, y_{s,M}^{RX}, \omega\right) \end{bmatrix},\ s = 1, \dots, S \tag{6}$$

is an array containing the samples of the scattered electric field at the M measurement points (being $\left(x_{s,m}^{RX}, y_{s,m}^{RX}\right)$, $m = 1, \dots, M$, their positions in the transverse plane) for the sth illumination, the vector:

$$\mathbf{e}_{tot}^{s} = \begin{bmatrix} e_{tot}^{s}(x_1^D, y_1^D, \omega) \\ \vdots \\ e_{tot}^{s}(x_N^D, y_N^D, \omega) \end{bmatrix} \tag{7}$$

is an array containing the values of total electric field in the centers $\left(x_i^D, y_i^D\right)$, $i = 1, \dots, N$, of the N subdomains used to discretize the investigation area, and:

$$\boldsymbol{\tau} = \begin{bmatrix} \tau(x_1^D, y_1^D) \\ \vdots \\ \tau(x_N^D, y_N^D) \end{bmatrix} \tag{8}$$

is an array containing the coefficients of the discretized contrast function. Finally, the matrix $\mathbf{H}^s$ is given by:

$$\mathbf{H}^{s} = j\frac{k_0^2}{4}\begin{bmatrix} h_{s,1,1} & \dots & h_{s,1,N} \\ \vdots & \ddots & \vdots \\ h_{s,M,1} & \dots & h_{s,M,N} \end{bmatrix},\ s = 1, \dots, S \tag{9}$$

whose elements are provided by the following relation:

$$h_{s,m,i} = \int_{D_i} H_0^{(2)}\left(k_0\rho_{s,m}\right)dx'dy' \tag{10}$$

being D_i the ith subdomain and $\rho_{s,m} = \sqrt{\left(x_{s,m}^{RX} - x'\right)^2 + \left(y_{s,m}^{RX} - y'\right)^2}$.

It is worth noting that the array $\mathbf{e}_{tot}^{s}$ is unknown into equation (5). Consequently, a second equation is needed to solve the inverse problem. Such relation is found by applying (3) to points inside the investigation area. By using the same discretization, we obtain the following matrix relation:

$$\mathbf{e}_{tot}^{s} = \mathbf{e}_{inc}^{s} - \mathbf{G}\mathrm{diag}(\boldsymbol{\tau})\mathbf{e}_{tot}^{s},\ s = 1, \dots, S \tag{11}$$

where:

$$\mathbf{e}_{inc}^{s} = \begin{bmatrix} e_{inc}^{s}(x_1^D, y_1^D, \omega) \\ \vdots \\ e_{inc}^{s}(x_N^D, y_N^D, \omega) \end{bmatrix},\ s = 1, \dots, S \tag{12}$$

is an array containing the values of the incident electric field in the centers of the N subdomains D_i. Moreover, the term:

$$\mathbf{G} = j\frac{k_0^2}{4}\begin{bmatrix} g_{1,1} & \cdots & g_{1,N} \\ \vdots & \ddots & \vdots \\ g_{N,1} & \cdots & g_{N,N} \end{bmatrix} \tag{13}$$

is a matrix whose elements are given by:

$$g_{i,k} = \int_{D_k} H_0^{(2)}(k_0\rho_i)dx'dy' \tag{14}$$

with $\rho_i = \sqrt{\left(x_i^D - x'\right)^2 + \left(y_i^D - y'\right)^2}$.

Equations (5) and (11) are combined together in order to obtain the following set of nonlinear equations:

$$\mathbf{e}_{scatt}^{s} = \mathbf{H}\mathrm{diag}(\boldsymbol{\tau})\left(\mathbf{I} - \mathbf{G}^{s}\mathrm{diag}(\boldsymbol{\tau})\right)^{-1}\mathbf{e}_{inc}^{s} = \mathbf{A}^{s}(\boldsymbol{\tau}),\ s = 1, \dots, S \tag{15}$$

which can be written as:

$$\mathbf{e}_{scatt} = \begin{bmatrix} \mathbf{e}_{scatt}^{1} \\ \vdots \\ \mathbf{e}_{scatt}^{S} \end{bmatrix} = \begin{bmatrix} \mathbf{A}^{1}(\boldsymbol{\tau}) \\ \vdots \\ \mathbf{A}^{S}(\boldsymbol{\tau}) \end{bmatrix} = \mathbf{A}\ \ (\boldsymbol{\tau}) \tag{16}$$

Equation (16) needs to be solved in order to retrieve the contrast function $\boldsymbol{\tau}$. Once this term is obtained, the distributions of the dielectric parameters can be calculated using equation (4). The solution of equation (16) represents however a highly ill-posed problem. Consequently, a regularized inversion algorithm must be used (Autieri, Ferraiuolo, & Pascazio, 2011; Lobel, Blanc-Féraud, Pichot, & Barlaud, 1997). The solving procedure is based on a two-step iterative strategy (Bozza et al., 2006; Estatico et al., 2005), in which an outer linearization is performed by means of an Inexact-Newton scheme and a regularized solution to the obtained linear system is calculated by means of a truncated Landweber algorithm (Landweber, 1951).

The developed iterative procedure works as follows.

1. Set iteration index to $n = 0$ and initialize the unknown $\boldsymbol{\tau}_n$, e.g., by choosing $\boldsymbol{\tau}_n = 0$;
2. Linearize the equation $\mathbf{e}_{scatt} = \mathbf{A}(\boldsymbol{\tau})$ in order to obtain a linear equation $\mathbf{J}_n\mathbf{h} = \mathbf{e}_n$, where $\mathbf{e}_{scatt} - \mathbf{A}(\boldsymbol{\tau}_n)$ and $\mathbf{J}_n$ is the Jacobian matrix (i.e., the discrete counterpart of the Frechét derivative) of $\mathbf{A}$ at point $\boldsymbol{\tau}_n$, which is given by (Remis & van den Berg, 2000):

$$\mathbf{J}_n = \begin{bmatrix} \mathbf{J}_n^1 \\ \vdots \\ \mathbf{J}_n^S \end{bmatrix} = \begin{bmatrix} \mathbf{H}_n^1 \mathrm{diag}\left(\mathbf{e}_{tot_n}^1\right) \\ \vdots \\ \mathbf{H}_n^S \mathrm{diag}\left(\mathbf{e}_{tot_n}^S\right) \end{bmatrix} \tag{17}$$

   being $\mathbf{e}_{tot_n}^s = \left(\mathbf{I} - \mathbf{G}\mathrm{diag}(\boldsymbol{\tau}_n)\right)^{-1}\mathbf{e}_{inc}^s$ the total electric field (for the sth illumination) inside the investigation area due to the current estimate of the solution $\boldsymbol{\tau}_n$ and $\mathbf{H}_n^s$ a inhomogeneous Green matrix given by $\mathbf{H}_n^s = \left(\mathbf{I} - \mathbf{G}\mathrm{diag}(\boldsymbol{\tau}_n)\right)^{-1}\mathbf{H}^s$;
3. Find a regularized solution $\mathbf{h}$ of the linearized equation by using a truncated Landweber algorithm;
4. Update current solution with $\boldsymbol{\tau}_{n+1} = \boldsymbol{\tau}_n + \mathbf{h}$;
5. Check if a convergence criteria (e.g., a maximum number of iterations n_{max} or a threshold on the residual) is fulfilled. Otherwise go back to step 2.

The truncated Landweber algorithm can be summarized as follows.

1. Set iteration index to $l = 0$ and initialize the unknown $\mathbf{h}_l = 0$;
2. Update the current solution with

$$\mathbf{h}_{l+1} = \mathbf{h}_l - \beta\mathbf{J}_n^*(\mathbf{J}_n\mathbf{h}_l - \mathbf{e}_n) \tag{18}$$

   where $\beta = 0.5/\|\mathbf{J}_n^*\mathbf{J}_n\|^2$ and $\mathbf{J}_n^*$ is the adjoint of $\mathbf{J}_n$;
3. Check if a convergence criteria (e.g., a maximum number of iterations, l_{max}, or a threshold on the residual) is fulfilled. Otherwise go back to step 2.

3. Imaging setup configuration and measurements

In order to prove the effectiveness of the approach, experimental validations are performed on a reference target by adopting the setup configuration in Fig. 2. A square investigation domain D around the scatterer is assumed, with a transmitting antenna giving an incident field oriented along the longitudinal axis of the target and assuming the positions indicated in Fig. 2 as black circles. A receiving antenna is adopted to collect the complex (amplitude and phase) field scattered by the test object on the void circles, at spacings Δx, Δy satisfying the Shannon's sampling theorem (Bucci & Franceschetti, 1989).

3.1. X-band measurements

The imaging configuration described in Fig. 2 is realized into the anechoic chamber of Microwave Laboratory at University of Calabria. Two standard X-band horn antennas are adopted as transmitting and receiving antennas, as providing a sufficiently large pattern

impinging on the reference target. This is given by a wood cylinder of length equal about to 60 cm (~ 20 λ @ 10 GHz) and square cross section of side equal about to 4 cm. A photograph showing the imaging setup is reported in Fig. 3.

Scattered field measurements are performed at a frequency equal to 10 GHz, on a square measurement domain of side equal to 39 cm, which has been discretized into $4M$ points ($M = 53$) with spacings $\Delta x = \Delta y = \lambda/4$. As highlighted above, both transmitting and receiving horns are oriented with the field parallel to the cylinder axis. The amplitude and phase behavior of the measured scattered field is reported in Figs. 4-7 for two different positions of the illuminating horn, along two different sides of the acquisition domain scanned by the receiving probe. The positions of transmitting and receiving antennas are visible in the picture within the same figures. Similar behaviors are obtained for the other positions of the transmitting and the receiving antennas.

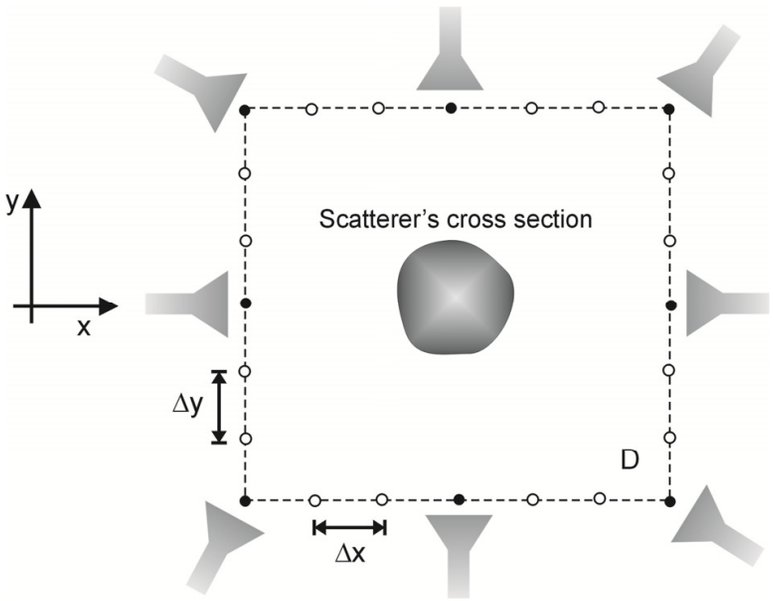

Figure 2. Imaging setup configuration

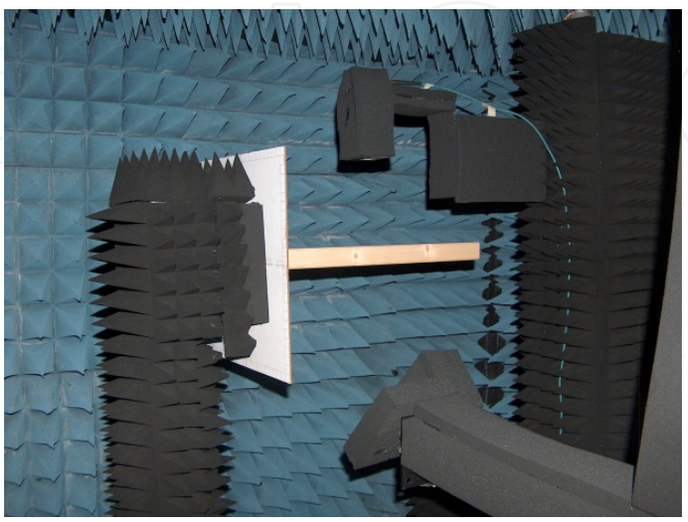

Figure 3. Photograph of measurement setup into the Microwave Laboratory at University of Calabria

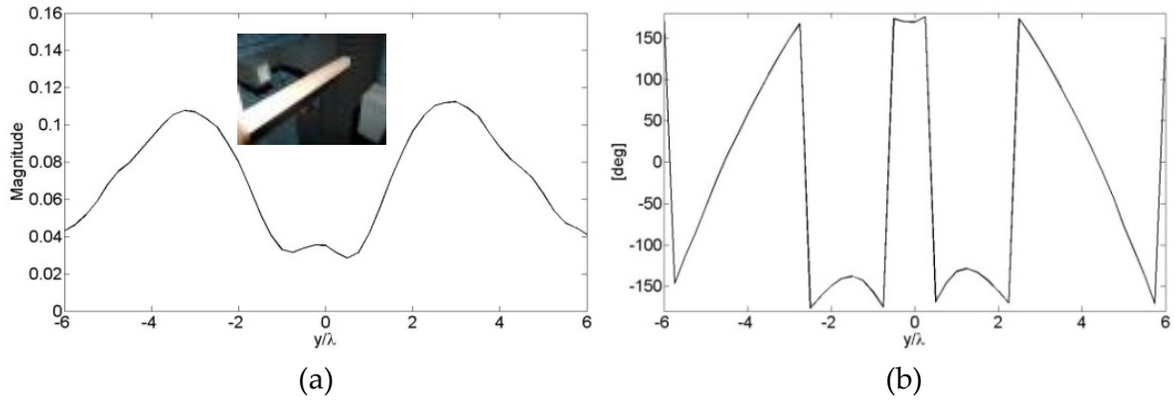

Figure 4. Amplitude (a) and phase (b) of measured scattered field: configuration in the picture

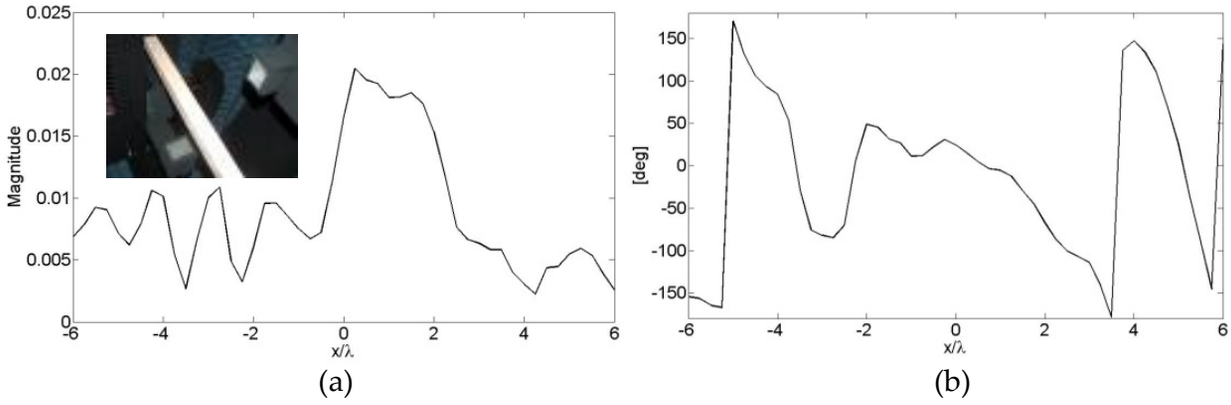

Figure 5. Amplitude (a) and phase (b) of measured scattered field: configuration in the picture

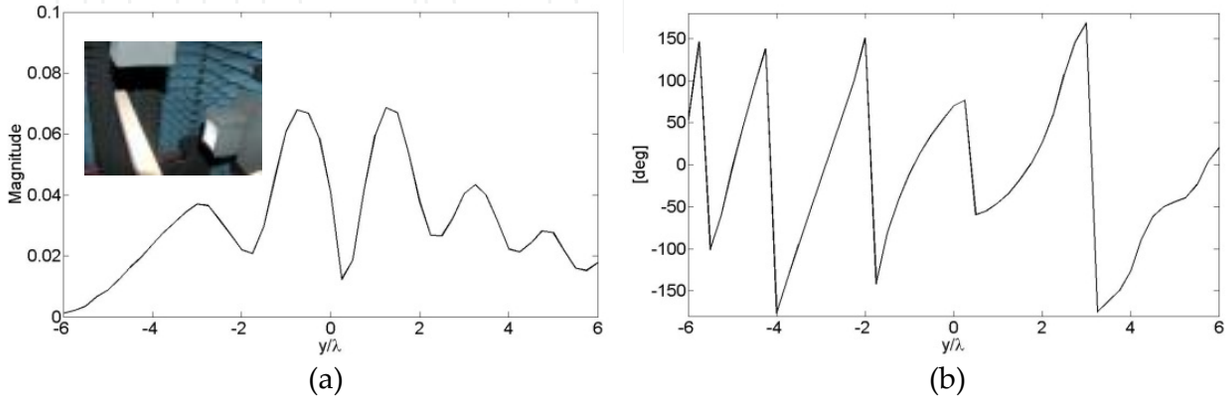

Figure 6. Amplitude (a) and phase (b) of measured scattered field: configuration in the picture

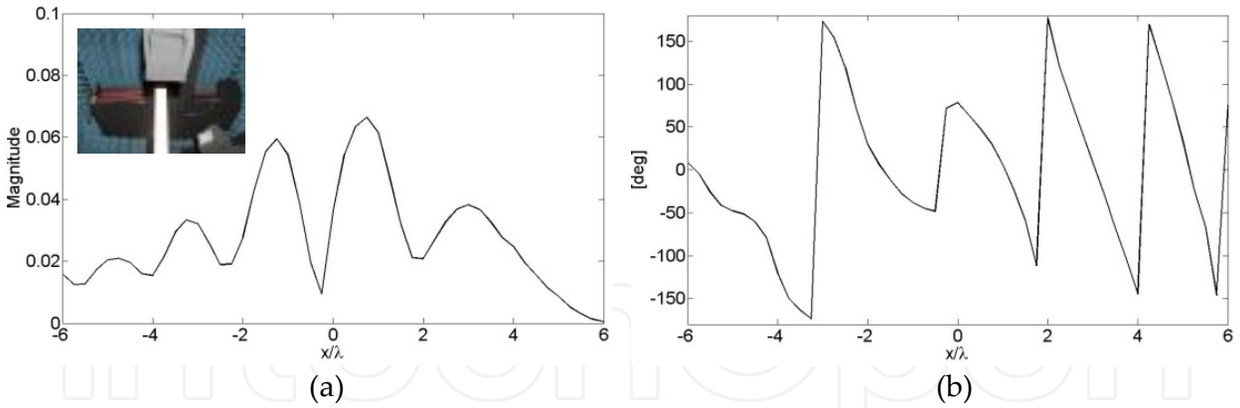

Figure 7. Amplitude (a) and phase (b) of measured scattered field: configuration in the picture

4. Preliminary reconstruction results

In this section, preliminary reconstruction results are reported. Figure 8 provides the reconstructed image of the object described in Section 3. It is obtained by inverting the real measured data described in Section 3 by using the procedure described in Section 2.

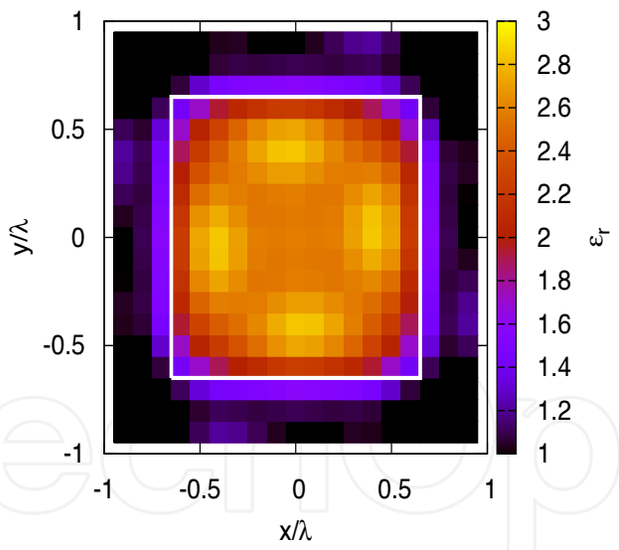

Figure 8. Reconstructed distribution of the relative dielectric permittivity inside the square investigation domain

For every side of the measurement domain, three positions of the TX antenna are used. In particular, for the first side (i.e., the one characterized by coordinate $x = -19.5\ cm$), the y-positions of TX antenna are equal to -3.625, 0, and 3.625 cm. For these three source positions, only the M measurement points located on the opposite side of the measurement domain (i.e., for the first side, those characterized by coordinate $x = 19.5\ cm$) are used. The

remaining views are constructed in a similar way. The total number of illuminations is $S = 12$ and the total number of measured samples is $S \times M = 636$. The investigation area is assumed of square shape and side equal to 0.06 m. It is partitioned into 20×20 square subdomains. The algorithm is initialized by using a rough estimate obtained by means of a back-propagation algorithm (Lobel, Kleinman, Pichot, Blanc-Feraud, & Barlaud, 1996). The inner loop (Landweber algorithm) is stopped after a fixed number of iterations $l_{max} = 5$. The outer loop (Newton linearization) is stopped according to the L-curve criteria (Vogel, 2002), leading to an estimated optimal number of outer iterations of $n_{lc} = 3$. Maximum, minimum and mean values of the retrieved dielectric permittivity distribution are reported in Table 1. Finally, Fig. 9 reports the profiles obtained by cutting the 2D distribution along two horizontal and vertical axes passing from the center of the investigation domain. As can be seen, the presence of the target can be suitably retrieved.

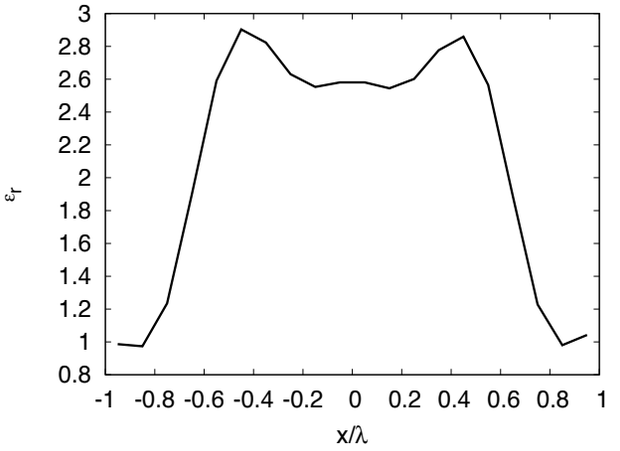

(a)

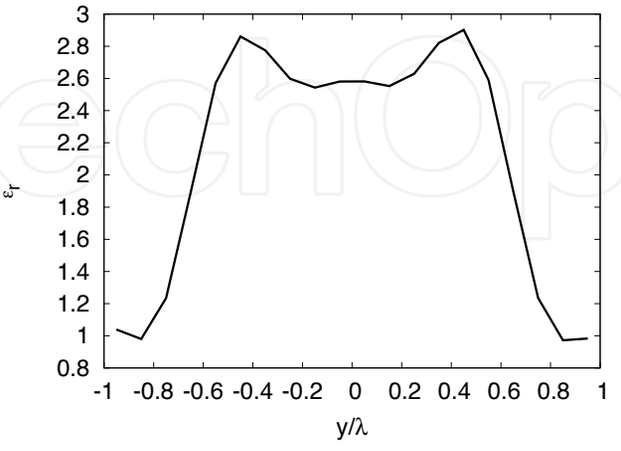

(b)

Figure 9. Horizontal and vertical profiles of the reconstructed distribution of the relative dielectric permittivity along lines passing from the center of the investigation domain

	Min	Max	Mean	Variance
Whole domain	1.00	2.90	1.67	0.48
Object	1.10	2.90	2.30	0.20
Background	1.00	1.41	1.08	0.01

Table 1. Values of the retrieved relative dielectric permittivity

5. Conclusion

The non-invasive inspection of dielectric objects has been considered in this Chapter to provide an accurate characterization of the permittivity profile at microwave frequencies. A mathematical formulation in terms of a Fredholm integral equation of the first order has been assumed, and a suitable discretization has been performed in order to numerically solve the resulting inverse problem, with a regularization approach adopted to overcome the intrinsic ill-posedness. The proposed imaging technique has been experimentally assessed by performing scattered field measurements on a square investigation domain surrounding a cylindrical dielectric target of known properties. Measured X-band data acquired by a standard horn antenna have been collected for different positions of the illuminating horn, and a successful reconstruction of the expected dielectric profile has been obtained from the application of the proposed technique.

Author details

Sandra Costanzo, Giuseppe Di Massa and Antonio Borgia
University of Calabria, Italy

Matteo Pastorino and Andrea Randazzo
University of Genoa, Italy

6. References

Ali, M. A., & Moghaddam, M. (2010). 3D Nonlinear Super-Resolution Microwave Inversion Technique Using Time-Domain Data. *IEEE Trans. Antennas Propag.*, Vol. 58, (2010) page numbers (2327–2336).

Autieri, R., Ferraiuolo, G., & Pascazio, V. (2011). Bayesian Regularization in Nonlinear Imaging: Reconstructions From Experimental Data in Nonlinearized Microwave Tomography. *IEEE Trans. Geosci. Remote Sens.*, Vol. 49, (2011) page numbers (801–813).

Bellizzi, G., Bucci, O. M., & Catapano, I. (2011). Microwave Cancer Imaging Exploiting Magnetic Nanoparticles as Contrast Agent. *IEEE Trans. Biomed. Eng.*, Vol. 58, (2011), page numbers (2528–2536).

Bozza, G., Estatico, C., Pastorino, M., & Randazzo, A. (2006). An Inexact Newton Method for Microwave Reconstruction of Strong Scatterers. *IEEE Antennas Wirel. Propag. Lett.*, Vol. 5, (2006) page numbers (61–64).

Bucci, Cardace, N., Crocco, L., & Isernia, T. (2001). Degree of Nonlinearity and A New Solution Procedure in Scalar Two-Dimensional Inverse Scattering Problems. *J. Opt. Soc. Am. A*, Vol. 18, (2001) page numbers (1832–1843).

Bucci, & Franceschetti, G. (1989). On the Degrees of Freedom of Scattered Fields. *IEEE Trans. Antennas Propag.*, Vol. 37, (1989) page numbers (918–926).

Catapano, I., Crocco, L., & Isernia, T. (2007). On Simple Methods for Shape Reconstruction of Unknown Scatterers. *IEEE Trans. Antennas Propag.*, Vol. 55, (2007) page numbers (1431-1436).

Chen, X. (2008). Signal-Subspace Method Approach to the Intensity-Only Electromagnetic Inverse Scattering Problem. *J. Opt. Soc. Am. A*, Vol. 25, (2008) page numbers (2018–2024).

Costanzo, S. & Di Massa, G. (2011). Advanced numerical techniques for near-field antenna measurements, In: *Numerical simulations of physical and engineering processes*, J. Awrejcewicz Ed., pp. (321-338), INTECH, ISBN 978-953-307-620-1, Croatia

El-Shenawee, M., Dorn, O., & Moscoso, M. (2009). An Adjoint-Field Technique for Shape Reconstruction of 3-D Penetrable Object Immersed in Lossy Medium. *IEEE Trans. Antennas Propag.*, Vol. 57, (2009) page numbers (520–534).

Estatico, C., Bozza, G., Massa, A., Pastorino, M., & Randazzo, A. (2005). A Two-Step Iterative Inexact-Newton Method for Electromagnetic Imaging of Dielectric Structures from Real Data. *Inv. Probl.*, Vol. 21, (2005) page numbers (S81–S94).

Ferraye, R., Dauvignac, J.-Y., & Pichot, C. (2003). An Inverse Scattering Method Based on Contour Deformations by Means of a Level Set Method Using Frequency Hopping Technique. *IEEE Trans. Antennas Propag.*, Vol. 51, (2003) page numbers (1100–1113).

Franchois, A., & Pichot, C. (1997). Microwave imaging-complex permittivity reconstruction with a Levenberg-Marquardt method. *IEEE Trans. Antennas Propag.*, Vol. 45, (1997), page numbers (203–215).

Gilmore, C., Mojabi, P., & LoVetri, J. (2009). Comparison of an Enhanced Distorted Born Iterative Method and the Multiplicative-Regularized Contrast Source Inversion method. *IEEE Trans. Antennas Propag.*, Vol. 57, (2009), page numbers (2341–2351).

Habashy, T. M., & Abubakar, A. (2004). A General Framework for Constraint Minimization for the Inversion of Electromagnetic Measurements. *Prog. Electromag. Res.*, Vol. 46, (2004) page numbers (265–312).

Isernia, T., Pascazio, V., & Pierri, R. (2001). On the local minima in a tomographic imaging technique. *IEEE Trans. Geosci. Remote Sens.*, Vol. 39, (2001) page numbers (1596–1607).

Kharkovsky, S., & Zoughi, R. (2007). Microwave and millimeter wave nondestructive testing and evaluation - Overview and recent advances. *IEEE Instrum. Meas. Mag.*, Vol. 10, (2007) page numbers (26–38).

Landweber, L. (1951). An Iteration Formula for Fredholm Integral Equations of the First Kind. *Am. J. Math.*, Vol. 73, (1951) page numbers (615–624).

Lesselier, D., & Bowler, J. (2002). Special section on electromagnetic and ultrasonic nondestructive evaluation. *Inv. Probl.*, Vol. 18, (2002).

Litman, A., Lesselier, D., & Santosa, F. (1998). Reconstruction of a two-dimensional binary obstacle by controlled evolution of a level-set. *Inv. Probl.*, Vol. 14, (1998) page numbers (685–706).

Lobel, P., Blanc-Féraud, L., Pichot, C., & Barlaud, M. (1997). A New Regularization Scheme for Inverse Scattering. Inverse Problems. *Inv. Probl.*, Vol. 13, (1997) page numbers (403–410).

Lobel, P., Kleinman, R. E., Pichot, C., Blanc-Feraud, L., & Barlaud, M. (1996). Conjugate-Gradient Method for Soliving Inverse Scattering with Experimental Data. *IEEE Antennas Propag. Mag.*, Vol. 38, (1996).

Oliveri, G., Lizzi, L., Pastorino, M., & Massa, A. (2012). A Nested Multi-Scaling Inexact-Newton Iterative Approach for Microwave Imaging. *IEEE Trans. Antennas Propag.*, Vol. 60, (2012), page numbers (971–983).

Pastorino, M. (2010). *Microwave imaging*. John Wiley, Hoboken N.J.

Paulsen, K. D., Poplack, S. P., Li, D., Fanning, M. W., & Meaney, P. M. (2000). A clinical prototype for active microwave imaging of the breast. *IEEE Trans. Microw. Theory Tech.*, Vol. 48, (2000), page numbers (1841–1853).

Rekanos, I. T. (2008). Shape Reconstruction of a Perfectly Conducting Scatterer Using Differential Evolution and Particle Swarm Optimization. *IEEE Trans. Geosci. Remote Sens.*, Vol. 46, (2008) page numbers (1967–1974).

Remis, R. F., & van den Berg, P. M. (2000). On the equivalence of the Newton-Kantorovich and distorted Born methods. *Inv. Probl.*, Vol. 16, (2000), page numbers (L1–L4).

Richmond, J. (1965). Scattering by a Dielectric Cylinder of Arbitrary Cross Section Shape. *IEEE Trans. Antennas Propag.*, Vol. 13, (1965) page numbers (334–341).

Rocca, P., Benedetti, M., Donelli, M., Franceschini, D., & Massa, A. (2009). Evolutionary Optimization as Applied to Inverse Scattering Problems. *Inv. Probl.*, Vol. 25, (2009).

Schilz, W., & Schiek, B. (1981). Microwave Systems for Industrial Measurements. *Advances in Electronics and Electron Physics*, pp. (309–381). Elsevier.

Shea, J. D., Kosmas, P., Van Veen, B. D., & Hagness, S. C. (2010). Contrast-Enhanced Microwave Imaging of Breast Tumors: A Computational Study Using 3D Realistic Numerical Phantoms. *Inv. Probl.*, Vol. 26, (2010).

van den Berg, P. M., & Abubakar, A. (2001). Contrast Source Inversion Method: State of Art. *Prog. Electromag. Res.*, Vol. 34, (2001) page numbers (189–218).

Vogel, C. R. (2002). *Computational methods for inverse problems*. Society for Industrial and Applied Mathematics, Philadelphia.

Zhang, Z. Q., & Liu, Q. H. (2004). Three-Dimensional Nonlinear Image Reconstruction for Microwave Biomedical Imaging. *IEEE Trans. Biomed. Eng.*, Vol. 51, (2004), page numbers (544–548).

Zhou, H., Takenaka, T., Johnson, J., & Tanaka, T. (2009). A Breast Imaging Model Using Microwaves and a Time Domain Three Dimensional Reconstruction Method. *Prog. Electromag. Res.*, Vol. 93, (2009) page numbers (57–70).

Zoughi, R. (2000). *Microwave Non-Destructive Testing and Evaluation*. Kluwer Academic Publishers, Dordrecht.

IntechOpen